Manufacturing of a next generation active twist helicopter rotor blade and experimental results of functionality test

Steffen Kalow* Dipl.-Ing
Bram van de Kamp* Dipl.-Ing
Christoph Balzarek* Dipl.-Ing
Johannes Riemenschneider* Dr.-Ing

*Institute of Composite Structures and Adaptive Systems
German Aerospace Center (DLR)
Braunschweig, Germany

ABSTRACT

Vibration and noise are omnipresent in a helicopter environment and therefore their reduction is an important goal in helicopter research. Actuators embedded into the skin of a helicopter rotor blade can produce a twist, which influences the propagation of the air turbulence. Hence, vibration and noise levels can be significantly reduced. An important issue during operation of a rotor blade are the centrifugal loads which affect the actuators and can cause a failure. Based on the German Aerospace Center (DLR) project STAR(Smart Twisting Active Rotor), the design of an active twist rotor blade has been adapted, such that the loads in the actuator system can be significantly reduced and furthermore distributed evenly. Besides a new actuator design, described in an earlier study of the authors, this paper focus on the use of carbon fiber composite for the spar and additional straps near to the trailing edge. This increases the durability of a new generation of active twist rotor blades, which is the basis for a specific and efficient use of the active twist technology. A first prototype of the new designed rotor blade has already been built. The design changes are addressed in this paper as well as the manufacturing process. Finally results of the numerical model are validated experimentally in the whirl tower and blade properties of the prototype blade are presented.

INTRODUCTION

The basic principle of individual blade control and its benefits for an improved aerodynamic behavior has been shown in many different studies (Ref. 1). The goals of helicopter research are vibration and noise reduction as well as performance improvement. Active twist rotors can actively contribute to this. Embedded in the skin of a rotor blade, piezoceramic actuators are able to twist the entire rotor blade and thus influence the propagation of air vortexes. The German Aerospace Center is investigating this technology since many years and built several model rotor blades. A history of these activities can be found in Refs. 2–4. In 2013 DLR was prepared for a wind tunnel test with a four-bladed, fully instrumented rotor within the project STAR. The STAR rotor represents a Mach-scaled and essentially dynamically scaled model rotor. The blade geometry and airfoil is similar to the Bo105 but they are arranged in an articulated hub. A pre-testing of the STAR rotor happened at the DLR rotor test hall in Braunschweig, Germany. The aim of this test had been the proof of functionality for the complete wind tunnel model with emphasis on active twist and blade performance. The results has been presented in Ref. 5. Shortly before the end of the pretest fatigue problems occurred and the wind tunnel test had to be canceled. Since then, DLR has been researching the causes of failure and creating a new rotor blade design that increases the durability. The results, presented for the first time at AHS 2016 in West Palm Beach (Ref. 6), showed that the integration of the actuators is a huge challenge, because the actuators are subject to considerable loads due to the centrifugal force, which are the main reason for the actuator failures. Based on these findings the actuator and the rotor blade design were completely revised so that the loads in the actuator system are be significantly reduced and furthermore distributed evenly. In addition to a new actuator design, the use of carbon fiber composite for the spar and additional straps near to the trailing edge increase the durability of a new generation of active twist rotor blades, which is the basis for a specific and efficient use of the active twist technology.

Presented at the AHS International 74th Annual Forum & Technology Display, Phoenix, Arizona, USA, May 14–17, 2018.

IMPROVED BLADE DESIGN

To understand why the actuators failed during the tests a detailed investigation of the failure mechanisms was mandatory. This was the starting point for creating an improved rotor blade design. There are two different approaches to achieving the goal of developing a more robust active twist rotor. One of them is the increase of the actuators robustness for a better durability under high loads. This is addressed by an improved actuator design themselve. The other approach comprises the reduction of the overall actuator strain, which results from the static and dynamic loads. In previous designs these actuator

strains were very high especially at the trailing edge. Simultaneously, all other constraints, concerning for example active twist, strength analysis and dynamic properties, still have to be considered and satisfied. Many properties depend on each other, thus an iterative approach is necessary to find a design meeting all given constraints. This shows that the requirements for active twist blades are significantly higher than for passive rotor blades.

Based on the these requirements, numerous simulations were carried out with the tool SaMaRA (Structural Modelling and Rotor Analysis), which was developed at DLR. It is a parametric finite element model to meet these partially conflicting requirements as part of a structural optimization framework. The blade properties of each design were analyzed and finally led to the new design.

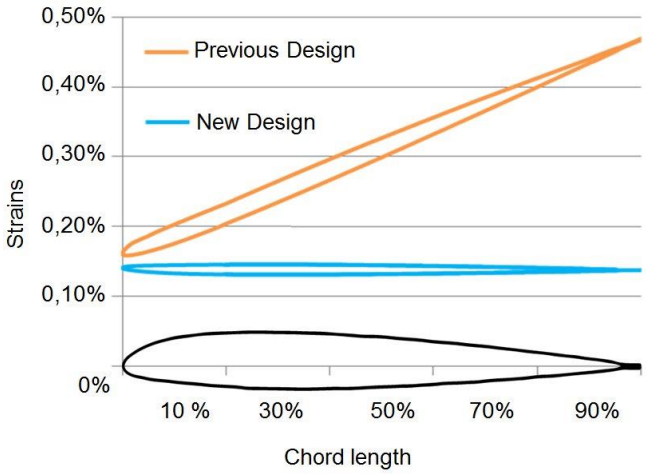

Fig. 1. Chordwise strain distribution near the blade root due to the centrifugal force.

Figure 1 shows the calculated strain distribution under pure centrifugal loads over the chord length for both designs. The orange curve represents the reference blade with an previous design from 2011 and shows that the strains at the trailing edge are much higher than the strains at the leading edge. The reason for this unequal distribution of loads was found in the position of the tension axis. If the positions the tension axis and the center of gravity of the blade do not match exactly, the blade deforms sickle-shaped under centrifugal loads. In this case, this means that the position of the tension axis was ahead the position of the center of gravity, which is at about a quarter of the chord length.

Therefore the rotor blade pivoted towards the leading edge. This lag bending led to very high loads in the actuators at the trailing edge, especially in the root area. Since the ceramics are very brittle high tensile stresses have fatal consequences. First cracks occur in the actuator ceramics. This leads to local strain concentrations in the electrodes and finally the electrodes fail. In Ref. 6 the failure mechanisms are shown and the allowable strain level for the actuators was identified.

Compared to the previous design, the improved blade design results in a completely different strain distribution. The simulation results suggest reduced and evenly distributed strains (blue curve in figure 1). The center of gravity and the tension axis are very close to each other.

Since the rotor blade shape originates from the BO105, its aerodynamic profile does not change over the radius. An active twist blade cross section including skin, actuators, spar, nose balance weight and cables for instrumentation is shown in figure 2. The upper cross section shows the previous design of 2011, the lower cross section shows the new design of 2016. The aerodynamic shape of the blades was not changed.

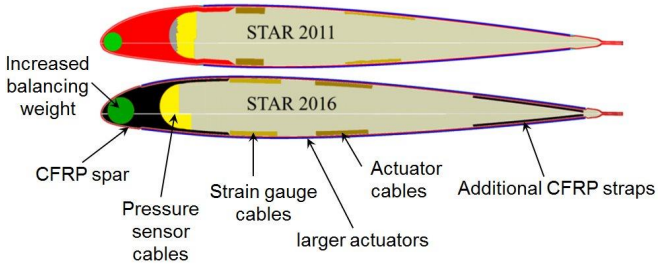

Fig. 2. Comparison of old and new rotorblade design.

The inner design on the other hand underwent some major changes which are presented here:

- A CFRP spar (black) with a reduced cross section by 35% and an increased tensile stiffness replaced the former GFRP spar (red)
- CRFP straps (black) near the trailing edge move the tension center in the direction of the trailing edge. The dimensioning of the straps provides a uniform elongation for the whole cross section under pure tension respectively the centrifugal loads
- The combination of both components reduces the strains under centrifugal force at the trailing by about 70% and the resulting elongation does not exceed 0.18% .
- Increasing the tensile stiffness also affects the lead lag and flap bending stiffness and increases it significantly
- Torsional stiffness remains nearly the same
- Due to the high instrumentation and the CFRP straps, the balancing weight had to be enlarged by a factor of 1.5, causing a 10% mass increase of the blade
- The CFRP straps also close the torsional box and thereby increases the induced twist

Table 1 gives a brief overview about the blade properties of both designs.

Table 1. Comparison of calculated blade parameters at r/R=0.25.

Characteristics	Design 2011	Design 2016
Lead Lag Bending Stiffness	7194 Nm	26500Nm
Flap Bending Stiffness	174 Nm	280Nm
Torsional Stiffness	169 Nm	172Nm
Tensile Stiffness	$1.35*10^7$ N	$2.95*10^7$ N
Center of Gravity	25.9 %chord	25.5 %chord
Tension Center	19.2 %chord	25.5 %chord
Mass per Length	1.32 kg/m	1.47 kg/m
Twist	5.4°	5.7°

The goal is to build a complete four-bladed rotor. Here, the reproducibility is another important requirement. All DLR active rotor blades are handmade and therefore unique. To ensure that all blades have the same characteristics, each blade will have an identical structure, although they will be instrumented differently. In the less equipped rotor blades sensors will be replaced by dummies and sensor cables will remain. Since the first set of STAR blades show different properties between the blades, this approach is chosen to minimize any deviation. Furthermore, an identical blade design contributes to a more standardized manufacturing process, which also adds to the objective of similar blades. To get an impression of the highly detailed models which were generated, figure 3 shows the skin with integrated actuators (dark brown for GFRP, lighter brown for the actuators) and the inner design with spar and straps made of carbon fiber (grey). Furthermore the pressure sensors (light brown) next to the cable tree in green and in a very dark grey the balancing weights at the leading edge are shown.

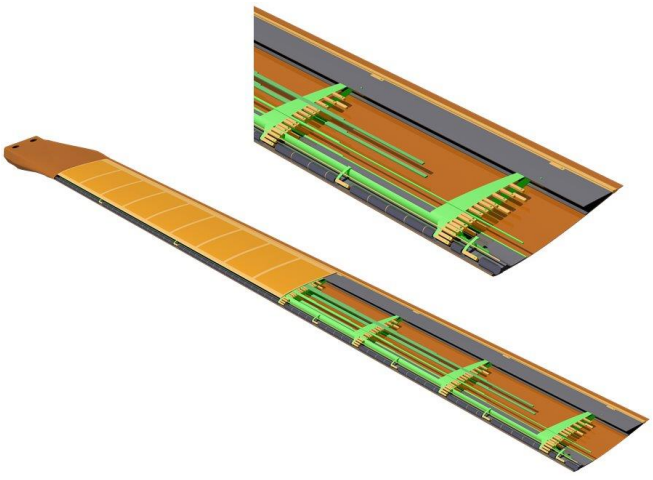

Fig. 3. Detailed rotor blade design, overall and detail

BLADE MANUFACTURING

The manufacturing process of highly instrumented rotor blades is very challenging. Due to the small size of the scaled blades, the manufacturing has to be very precise and allows only very little deviation in comparison to the CAD design. Especially the properties regarding stiffness and center of gravity have to meet the calculated ones. As already mentioned, the reproducibility is also a big issue that has to be solved. In STAR there were partially large deviations between the individual blades, which are partly attributable to the thermal shrinkage, amounts of adhesive or different instrumentation. Due to the new design additionally a combination of glass fiber components and carbon fiber components is used, such as it has not been used in active blades at DLR before. This represents new challenges as well. The requirement to build 5 blades with similar properties has a very high priority. Among other things, this requires the same work steps to be carried out in all blades by a consistent manufacturing team, since different ways of working can have a significant impact on the blade properties (e.g., mass and stiffness distribution) and thus flutter stability or blade comparability would not be guaranteed. Therefore, a detailled manufacturing schedule was developed comply with specified manufacturing steps in accordance to a standardized process. Furthermore, the integrity of the actuators must be ensured at all times until the completion of the manufacturing process. Numerous preliminary tests and maximum care in dealing with the sensitive actuators are a prerequisite for this.

Manufacturing of a prototype blade

A first prototype of the new designed rotor blade has already been built in mid-2017. The manufacturing process is explained below. The rotor blade is manufactured in two mold halves and at the end of the process both halves are glued together. The general manufacturing concept includes a lot of individual steps, but can be roughly summarized as follows:

1. Manufacturing of the skins with integrated actuators, strain gauges and wiring
2. Manufactoring of additional carbon fiber straps
3. Milling the spar out of a CFRP-plate and milling out the foam core segments
4. Gluing of CFRP-straps, sensors and spar
5. Cable positioning, soldering and shielding
6. Adaption of foam to the inner skin structure (cables, straps)
7. Gluing of counter weights in the spar
8. Final assembly of mold halves using adhesive
9. Finishing works (electrical connectors,)

The manufacturing of the skin is one of the most challenging tasks within the blade manufacturing as the actuators, sensors and wires are directly integrated. There are 15 actuators and 25 strain gauges (9 for torsion, 9 for flap and 7 for lag) integrated into each skin half (see figure 4). The skin consists of 2 layers of GFRP (Hexply913 - Prepreg material) and is cured in an autoclave. The use of prepreg provides high quality laminates with a predetermined and reproducible resin to fiber ratio.

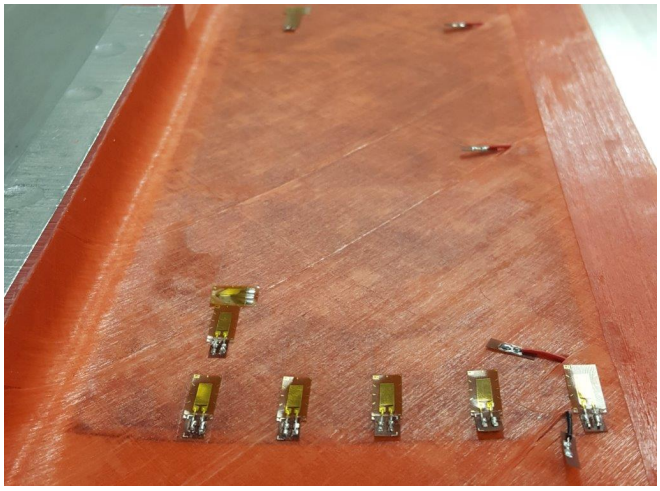

Fig. 4. Blade skin half with integrated actuators, strain gauges and wiring

The first steps in the skin manufacturing process are the cleaning of the aluminum molds and treatment with the release agent WaterWorks so that the blade can be demolded at the end of the manufacturing process. Subsequently, the individual actuators can be positioned and fixated in the molds. Since the release agent greatly reduces the adhesion on the mold surface, a defined positioning of the actuators is hardly possible. Remedy here is the solvent-free molding material placement aid PregMagic. This is applied selectively to the mold and generates the necessary adhesion for positioning the actuators. Subsequently, the two Prepreg fiber layers of the skin can be draped into the mold and onto the actuators. The skin consists of a +45 and a -45 degree layer and is reinforced at the trailing edge with a layer in the radial direction. As can be seen in figure 4, the cables of the actuators are then threaded through the prepreg and the strain gauges are placed in their respective position. This is followed by a layer of tear-off fabric and then the vacuum assembly can take place. Finally, both halves of the skin are hardened step by step in a microwave autoclave at 125°C. Figure 5 shows the finished skin after the curing process.

Like mentioned before, additional carbon fiber (M21E) straps are placed near to the trailing edge to reduce the radial strain affecting the actuators. The straps consist of 5 layers of CFRP with a width of 25.6mm and a total thickness of 0.65mm and were manufactured separately in the molds before manufacturing the skins. After finishing the skins they

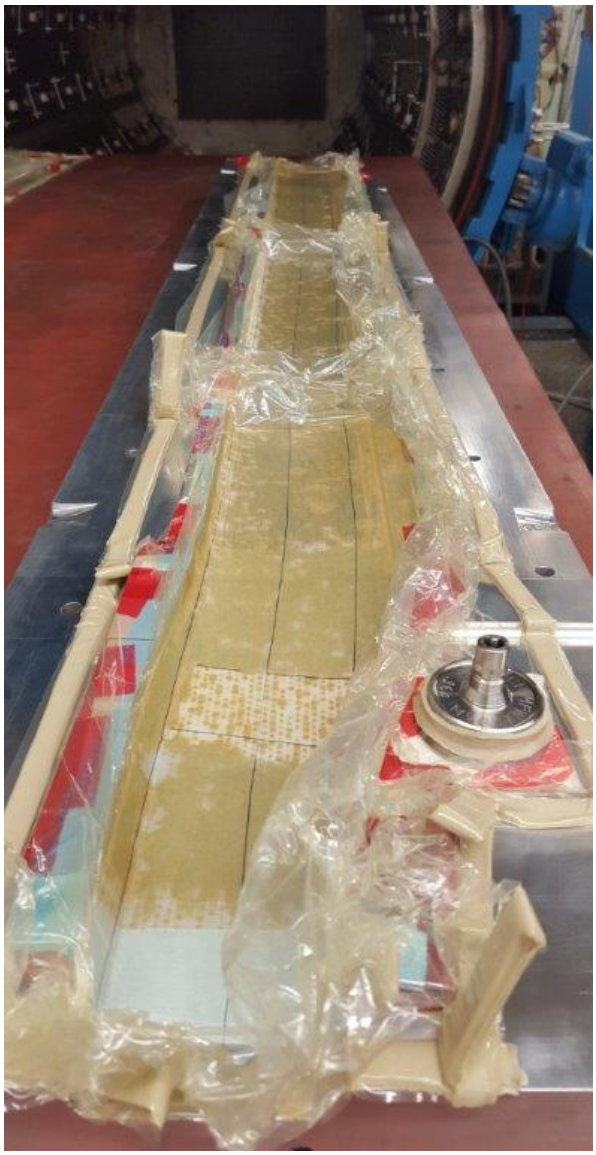

Fig. 5. Blade skin half after curing

are glued together under vacuum with the two component epoxy ARALDITE 2011. In this case, a corridor is marked at the respective position near the trailing edge and then adhesive is applied in a defined manner with a toothed (figure 6). The amount of applied adhesive is controlled by weight.

Various 3d printed templates are used in order to exactly position of the pressure sensors within the skin. They help to maintain the exact distances between the sensors, but also to place the cables (see figure 7). This is necessary to protect the sensors of breaking away or other damages during the gluing process of the spar. For the first prototype blade only dummies have been used which are intended to represent the masses of the expensive pressure sensors. All dummy masses were provided with cables in order to obtain the same characteristics as the fully instrumented rotor blades manufactured later on. Furthermore, the manufacturing process could be practiced and improved.

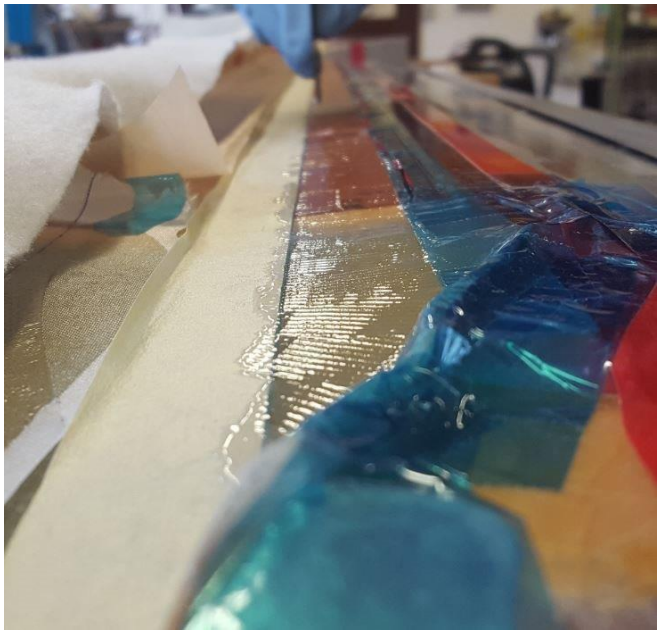

Fig. 6. Gluing process of trailing edge straps

Fig. 7. Positioning of pressure sensors

The same carbon fiber material is used for the spar. According to a layer plan numerous CFRP layers are stacked such that the root region has quasi-isotropic properties and the aerodynamic region has unidirectional properties. With this stack up a plate is manufactured. Afterwards, the complete spar contour is milled. Pressure sensor locations are omitted in the spar. The sensor cables are guided directly through the spar by a small notch and opening (see figure 8). This is necessary because in contrast to previous designs, the core and belt of the spar are no longer manufactured separately from each other. In previous rotor blades the spar was made of glass fiber composite and the Prepreg layers of the belt were cured in one step together with the skin layers. To minimize the risk through diverging thermal expansions for the sensitive and expensive rotor blade skin such a procedure with a mixture of carbon and glass fiber has been rejected.

At the lower left edge of figure 8 a kind of tongue at the spar can be seen. These are mounting points, three in total, to achieve improved positioning accuracy. With these mounting points, both the skin and the spar are fixed to small sleds with a radial degree of freedom. This radial degree of freedom enables the skin to extend while being cured and shrink while cooling down. For the gluing of the spar this degree of freedom blocked and a very precise positioning of the spar is ensured. This step is one of the most complex in the entire manufacturing process. First of all, all cables of the sensors, which are under the spar, have to be threaded through the small opening in the spar. Similar to the bonding of the CFRP straps near the trailing edges, the position of the spar is marked on the blade side and then applied to both the skin and the spar adhesive with the toothed spatula. Again, the amounts of adhesive are defined by their weight. Now the spar is positioned very carefully onto the skin. If the spar is perfectly positioned it can be fixated on the skin with clamps. Additionally a vacuum ensures uniform contact pressure (figure 9).

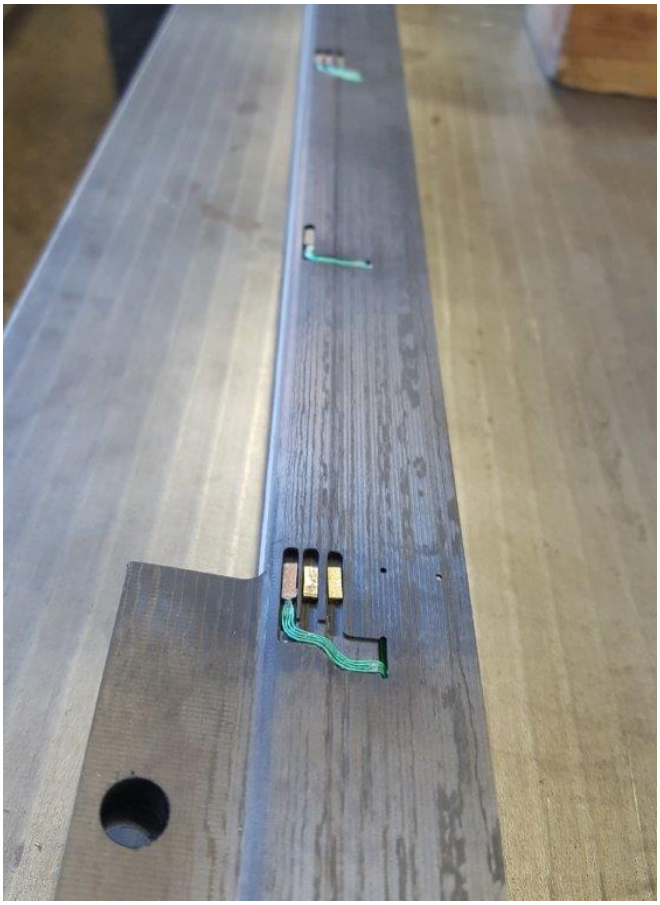

Fig. 8. Carbon fiber spar with integrated pressure sensor dummys

Since not all rotor blades can be equipped with the maximum number of sensors. In less instrumented blades sensor dummies replace the pressure sensors. The number of cables remains the same, which is resulting in a huge number of sensor cables. In the highest instrumented rotor blade, nearly 100 pressure sensors are to be installed. Each pressure sensor includes 4 cables. This means that, along with the cables of the

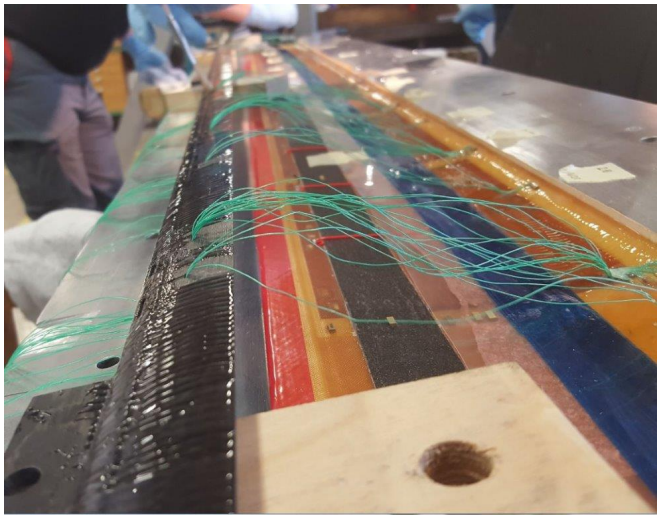

Fig. 9. Gluing of carbon fiber spar

strain gauges and the actuators, over 550 cables with a total length of more than 600 m have to be integrated in a very limited assembly space. This is an enormous challenge.

Due to the large amount of cables which have to be integrated in all rotor blades, the individual cables are pre-assembled, combined and manufactured as ribbon cables (see figure 10). These ribbon cables can be precisely positioned with a still high but significantly reduced effort. For handling the cables and gluing them with a thin adhesive layer tools to facilitate the exact placement of the cables are used (figure 11).

Fig. 10. Manufacturing of ribbon cables

Figure 12 shows the finished placement of all cables. The cables of the pressure sensors (green), strain gauges (multicolored) and the actuators (red) were separated from each other. Experiences from previous projects (see Ref. 6) have shown that the high voltage cables of the actuators influence the sensor signals. For this reason, all cables are inserted into a copper mesh in order to minimize electromagnetic interferences. The position of the individual cable assemblies is a compromise between the EMI problem and the mechanical properties, e.g. the position of the center of gravity. Furthermore, in figure 12 the carbon fiber reinforcement near the trailing

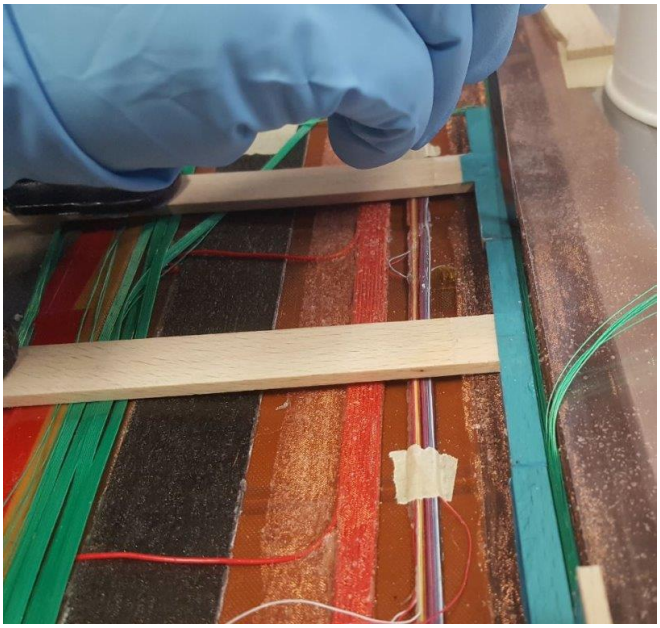

Fig. 11. Positioning aids for sensor cables

Fig. 12. Finished cabeling and shielding

edge is easily visible. Worthwhile to notice are the connection points of the actuators. These must be absolutely insulated from the electrically conductive carbon fiber reinforcement.

The foam parts, which have already been milled in shape, are brought into their final contour through manual adjustment. This means, the reinforced carbon straps routing of the cables or other unevenness must be removed from the foam if not sufficiently done in the milling process before they are finally glued into the mold halves. Then the parting plane can be milled. Subsequently the balancing weights can be inserted into the leading edge and glued with epoxy. Finally, both mold halves are glued together. After demolding, the final works on the outer contour are following, for example, drilling the bolt holes into the root or integrating LEDs into the blade tip.

The last challenge is the cabling in the connector housing. All sensors and actuators must be soldered to a variety of plugs. Figure 13 gives an overview of the complexity and effort behind this step. For the sensors, a special circuit board is used. A specially designed amplifier card sends the amplified sig-

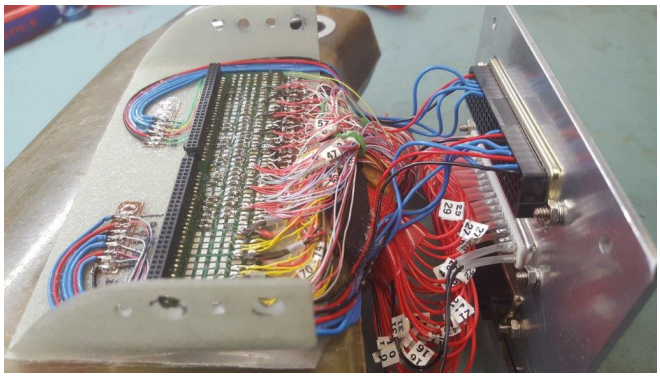

Fig. 13. Wiring at the blade root

nals from the rotor blade to the non-rotating system. Aluminum heat sink plates in the GFRP housing dissipate the heat of the amplifier cards to the outside.

The manufacturing of the first rotor blade prototype based on the new design was finished in the middle of 2017 and subsequently tested in the laboratory. Finally it is investigated in the whirl tower of the DLR in Brauschweig. Some parts of the results are presented in the following chapter.

EXPERIMENTAL EVALUATION OF STRUCTURAL BLADE PROPERTIES

The newly designed rotor blade is experimentally tested regarding structural properties and results are compared to the previously tested STAR rotor blades (Refs. 5, 7). The test setups are nearly identical between old and new measurements. The following properties regarding the airfoil region are measured and compared:

- Torsional stiffness
- Flap bending stiffness
- Chordwise position of the elastic axis
- Active twist angle with actuators

Measurement of torsional and flap bending stiffness as well as elastic axis

Torsional and flap bending stiffness as well as the elastic axis are determined in the laboratory for the airfoil region between its initial radial position and the end of the actuator area. Segments with modifications of the cross section due to implemented pressure sensors and contacts are considered to be of small radial extension compared to the blade length. Consequently, the structural properties are determined based on the assumption that the blades possess a uniform cross section design over the regarded region. Accordingly, the obtained structural properties represent averaged values.

Test setup

The first three properties were determined in one test setup. The blade is clamped at the bolts and hold in an upward position as shown in the left picture of figure 14. Additionally, it was fixed at the beginning of the airfoil region using an airfoil shaped clamp (figure 14, right). The blade was then loaded like a single side supported beam by an external force at the end of the actuator area within the airfoil region. Therefore, another clamp was mounted at the end of the actuator area near to the blade tip. The clamp was extended in chordwise direction such that it could be used as a lever for force application. The leading edge of the profile was defined as zero on the lever.

Fig. 14. left: Test rig with rotor blade; right: Rotor blade camp

The force was applied perpendicular to the radial blade axis and the clamp at the end of the actuator by a string. The string was pulled by an excenter rotating with 0.3 HZ to avoid creeping effects of the glass fiber composite material of the rotor blade. At the other end the string was attached to a load cell, to relate the displacements to their corresponding forces. The point of application of the force can be changed along the lever.

The blade deformation was measured with a photogrammetric system for the STAR blades and with a laser profile scanner for the prototype blade. Both systems can determine the in

plane movement of the clamp perpendicular to the spanwise direction. A schematic of the test setup is shown in figure 15

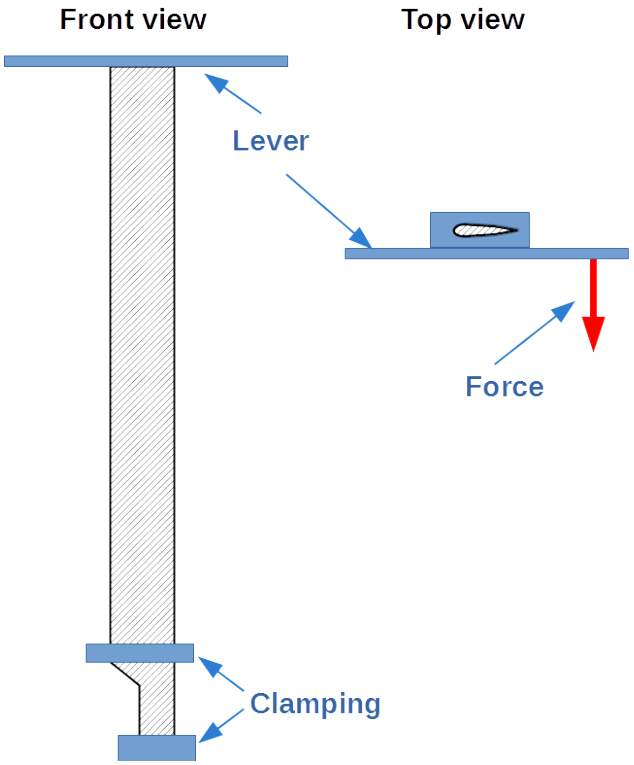

Fig. 15. Test setup schematic

Calculating stiffness and elastic axis from in plane deformation and force

In order to calculate the desired properties from the in plane movements of the clamp it was taken into account that any force F applied to the cross section is equivalent to the same force applied to the elastic axis combined with a moment F· d as shown in figure 16.

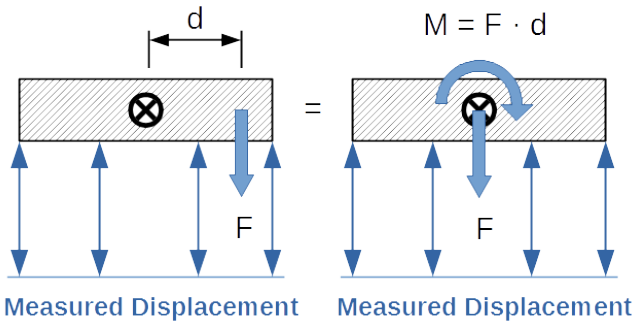

Fig. 16. Measuring and Calculation schematic

Accordingly resulting displacements w in profile thickness direction with varying force application points along the clamp and lever were measured.

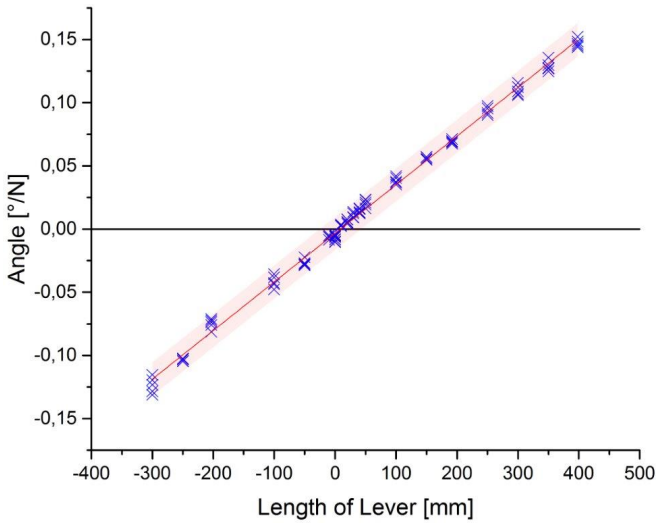

Fig. 17. Lever Displacements

The position of the elastic axis and thus length d is unknown. Therefore the data was used to calculate an angle of rotation. By interpolation the position with no rotational angle and thus a zero moment M could be determined, shown in figure 17.

As a zero moment M can only be obtained when d is zero. The elastic axis of the rotor blade is the point in figure 17 where the linear regression of angle and length of lever cross the $0/N$-axis. Knowing the position of the elastic axis, the applied moment M was derived for every single measurement and then related to the rotational angle vartheta and the length l between the clampings, resulting in the torsional stiffness GI of the rotorblade:

$$GI_T = \frac{M_T l}{\vartheta_l}$$

Likewise the displacement w was derived at the position of the elastic axis for every single measurement and correlated to the force F and the length l between the clampings, resulting in the flap bending stiffness EI:

$$EI_{flap} = \frac{l^3 \cdot F}{3 \cdot w}$$

Results and Discussion

Using the test set-up decribed in the previous section, the position of the elastic axis can be determined. For the prototype blade the linear regression is shown in figure 17 resulting in an position of 10,54 mm from the leading edge which translates to 8,7% chord length. A comparison of the elastic axis of STAR rotor blades with the prototype blade is given in figure 18.

The chordwise position of the elastic axis matches roughly that of the alpha and beta blade and lays far in front of the gamma, delta and epsilon blade. The prototype blade, alpha

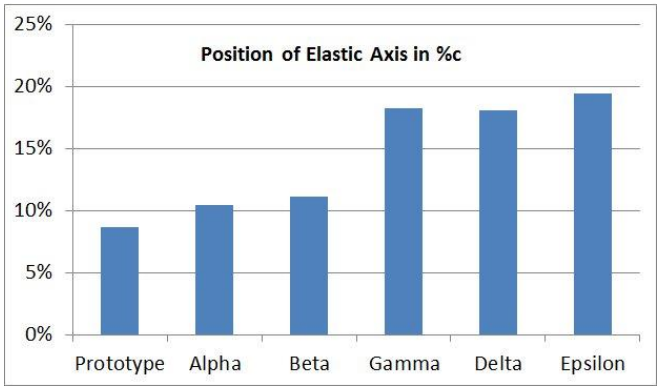

Fig. 18. Comparison of elastic axis positioning between new and old design

and beta have in common, that they all have integrated cables for a high grade of instrumentation. Most of these cables are positioned at the c-shape of the spar. With this positioning near to the leading edge the elastic axis moves in this direction, too. For the prototype blade the even higher cable amount and the stiffness cause the elastic axis to move forward even more.

Figure 19 shows a higher overall torsional stiffness in comparison to the alpha and beta blade. The other three blades will not be considered in this case, because of their low instrumentation grade. The higher stiffness of the prototype blade is caused by the stiffer spar and the additional carbon fiber straps at the trailing edge.

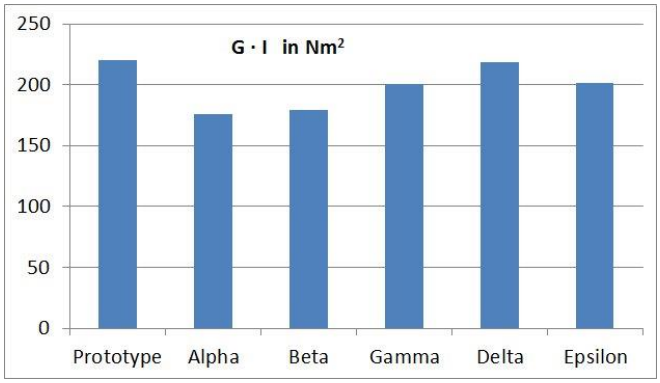

Fig. 19. Comparison of torsional stiffness between new and old design

A comparison of flap bending and torsional stiffness is given in figure 19 and figure 20. It can be seen, that the magnitude of the torsional stiffness of the prototype blade is nearly the same as the stiffest STAR blade (delta). The flap bending stiffness of the prototype blade however, is about 1.7 times greater than the stiffest of the STAR blades. This is due to the fact that carbon fiber is integrated into the truss and the trailing-edge strap to increase lag bending and tensile stiffness, which also increases flap bending stiffness.

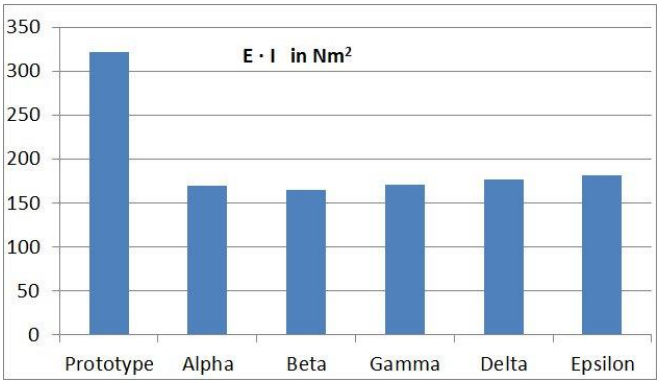

Fig. 20. Comparison of flap bending stiffness between new and old design

Measurement of Active Twist Angle

Lastly the active twist angle is measured. The same setup as for the stiffness measurements is used with the exception that the rotor blade is solely clamped at the bolts. Again the angle for the STAR blades was measured with a photogrammetry system, while the prototype blade was measured with a laser profile scanner. As can be seen in figure 21 the active twist is near the mean of the values of the STAR blades.

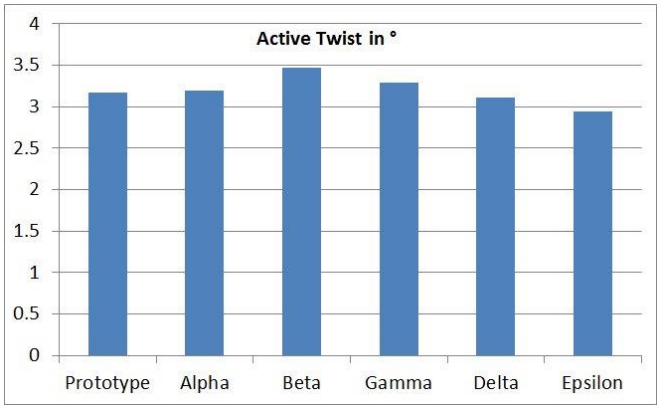

Fig. 21. Comparison of active twist between new and old design

Results and Discussion

Despite the fact, that the overall torsion stiffness is higher than for the alpha and beta blade the active twist remains at a similar value. Most of the actuator region does not suffer a higher local stiffness and thus the influence on the actuator elongation is small. Because of the additional closing of the torsional box at the trailing edge by the carbon straps, the actuator movement is transformed into a twist movement more efficiently.

WHIRLTOWER TESTS

The laboratory results have been very promising since the expectations on the new blade design were met. This was followed by numerous investigations under centrifugal loads in the whirl tower in Braunschweig. Finally it was the most comprehensive test matrix of all ever tested active twist blades in the whirl tower. After installing the prototype blade in the test rig, the speed was constantly increased in 100rpm steps to the nominal speed of 1043rpm. On the one hand this was used to balance the rotor system and on the other hand the condition of the actuators could be documented after each speed configuration. Furthermore, it was possible to observe how the blade behaves under increasing centrifugal loads regarding to the pivoting moments.

Fig. 22. Investigations of the efficiency of the prototype blade design in centrifugal test rig

In total, the rotor blade was tested for more than 50 hours under centrifugal loads. At the same time, the actuators were excited permanently in order to generate a continuous load. The comprehensive test matrix included regular reviews of the following aspects:

- natural frequency estimate
- strain distribution under centrifugal loads
- twist-performance
- durability

A detailed analysis of the data is still pending. However the first results of the natural frequency analysis show that no problems are to be expected regarding the flutter stability. The evaluation of the strain distribution showed a drastically reduced strain due to centrifugal loads with a very good comformity to the simulation results.

In the experiment strain distributions are measured at several radial positions and different rotor speeds. Figure 23 shows a comparison of the strains at the innermost aerodynamic section at nominal speed. Furthermore, it can be clearly seen that

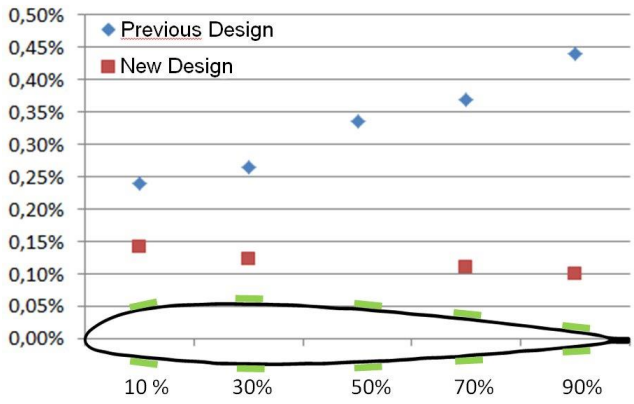

Fig. 23. Strain distribution of previous and new design at innermost cross-section of the aerodynamic profil

the design changes have an enormous effect on the strain distribution. While the strains at the leading edge have dropped 60%, the trailing edge strains have been reduced more than fourfold. As expected the position of the tension axis is close to the center of gravity. In comparision to the previous design the axis is even behind the center of gravity. This results in a small pivoting deflection to the trailing edge, which leads to a compressive preload of the actuators at the trailing edge region. This has also a positive effect on the durability of the actuators.

In summary, it can be shown that all measures for a drastically reduction of the strains take effect. In particular, the use of CFRP for the spar and the use of additional reinforced layers have a decisive influence. In combination with the improved actuator design, sufficient durability of the actuators for the planned wind tunnel period could be demonstrated. A performance loss by the actuators over a period of more than 50 operating hours could not be noticed. There was also no increased incidence of burn through or other abnormalities that could hinder the planned wind tunnel test.

Table 2. Twist Performance at harmonic excitation.

Harmonic excitation	Excitation voltage	Twist angle [pp]
0/rev (0.15Hz)	50%	3.2°
1/rev (17.5Hz)	70%	3.0°
2/rev (35.0Hz)	65%	4.0°
3/rev (52.0Hz)	30%	4.0°
4/rev (69.5Hz)	70%	4.0°
5/rev (87.2Hz)	60%	2.5°
6/rev (104.2Hz)	50%	1.5°

For the successful execution of the wind tunnel tests 4° peak-to-peak have been assumed for both quasi-static contol and 2/rev to 4/rev. Furthermore, 2° peak-to-peak should be achieved for 5/rev and 6/rev. In order to protect the actuators, not all configurations have been carried out to the maximum excitation. Very positive is that, depending on the excitation, a maximum of 70% of the total actuator power is already sufficient to meet the minimum requirements for twist perfor-

mance. Table 2 shows the maximum excited voltage in the experiment and compares the achieved twist angle. A reduced excitation voltage during the wind tunnel tests also has a positive effect on the load and thus the durability of the actuators.

CONCLUSION AND OUTLOOK

The actuators embedded in an active twist rotor blade are subject to considerable loads due to the high centrifugal force. Based on the DLR project STAR (Ref. 6), an active rotor design has been completly revised. The new design includes several material and structural adjustments. A revised actuator design is applied. The loads in the actuator system were significantly reduced to a noncritical amount and furthermore distributed evenly by using carbon fiber composite for the spar and placed additional straps near to the trailing edge. Hereby, most likely the fatigue problems of the actuators will be overcome. Furthermore manufacturing aspects have been presented within this paper. An important objective is the similarity of the individual rotor blades and its properties. To achieve this and due to the high requirements as well as the limited assembly space a detailed manufacturing concept is vital. Even though high effort was put into this, many challenges throughout the manufacturing process arose and had to be solved. The manufacturing of a rotor blade prototype was finished in the middle of 2017 and proved to be very useful as a basis for manufacturing the complete rotor blade set. The experimental results validate the simulations in most aspects and are as such very promising. Numerous investigations under centrifugal force were carried out in the whirl tower in Braunschweig.

First results of the natural frequency analysis show that no problems are to be expected regarding the flutter stability. The evaluation of the strain distribution showed drastically reduced strains due to blade dynamics and centrifugal loading. A sufficient durability of the actuator has been demonstrated, without any performance loss after more than 50 operating hours. Furthermore, the load on the actuators can be reduced since the minimum requirements for the twist performance are already met with a maximum of 70% of the actuator excitation.

Due to the positive results, the DLR will manufacture a complete set of blades for the next generation of active twist rotors based on the model of the prototype blade. The planning for this has already been completed and preliminary work are already started. At the same time, a new consortium with international partners is being formed, within the planned wind tunnel test can take place.

REFERENCES

[1]Maucher, C. K., Grohmann, B. A., and Junker, P., "Review of adaptive helicopter rotor blade actuation concepts," Adaptronic Congress, 2006.

[2]Monner, H. P., Opitz, S., Riemenschneider, J., and Wierach, P., "Evolution of Active Twist Rotor Designs at DLR," 49th AIAA/ASME/ASCE/AHS/ASC Structures, Structural Dynamics, and Materials Conference, April 2008.

[3]Monner, H. P., Riemenschneider, J., Opitz, S., and Schulz, M., "Development of active twist rotors at the German Aerospace Center (DLR)," 16th AIAA/ASME/AHS Adaptive Structures Conference, April 2011.

[4]Wierach, P., Riemenschneider, J., Opitz, S., and Hoffmann, F., "Experimental Investigation of an Active Twist Model Rotor Blade under Centrifugal Loads," EFR 2007, September 2007.

[5]Hoffmann, F., Schneider, O., van der Wall, B. G., Keimer, R., Kalow, S., Bauknecht, A., Ewers, B., Pengel, K., and Feenstra, G., "STAR Hovering Test - Proof of Functionality and Representative Results -," Paper 10-B in Conference Proceedings online, 40th European Rotorcraft Forum, September 2014.

[6]Kalow, S., Opitz, S., Riemenschneider, J., and Hoffmann, F., "Results of a parametric design study to adapt the structural properties and strain distribution of active twist blades," AHS 2016, Mai 2016.

[7]Riemenschneider, J., Keimer, R., and Kalow, S., "Experimental Bench Testing of an Active-Twist Rotor," ERF (European Rotorcrat Forum), September 2013.